



# Two-Dimensional Discrepancies in Fracture Geometric Factors and Connectivity Between Field-Collected and Stochastically Modeled DFNs: A Case Study of Sluice Foundation Rock Mass in Datengxia, China

Wen Zhang<sup>1,2</sup> · Rui Fu<sup>1</sup> · Chun Tan<sup>3,4</sup> · Zhifa Ma<sup>3,4</sup> · Ying Zhang<sup>5</sup> · Shengyuan Song<sup>1</sup> · Peihua Xu<sup>1</sup> · Shuonan Wang<sup>1</sup> · Yunpeng Zhao<sup>1</sup>

Received: 6 June 2019 / Accepted: 5 December 2019 / Published online: 29 January 2020  
© Springer-Verlag GmbH Austria, part of Springer Nature 2020

## Abstract

This study takes sluice foundation rock mass in Datengxia Hydropower Station, China as an example to examine two-dimensional (2D) discrepancies in fracture geometric factors and connectivity between field-collected and stochastically modeled discrete fracture networks (DFNs). We discover that the trace lengths of field-collected and corresponding modeled DFNs diverge, especially with relatively large lengths. A new variable called minimum spacing sequence (MSS) is proposed, which lists minimum spacing between each fracture midpoint and all the other fracture midpoints. The probability density function curve of MSS shows that the fracture locations do not follow a homogeneous (Poisson) model. The following is performed to examine whether the differences will result in noticeable DFN application errors. The 2D fracture connectivity, which is calculated by depth-first search algorithm, is applied to quantify the discrepancies between field-collected and statistically modeled 2D DFNs. Results show that the statistically modeled DFNs have small clustered fracture path numbers and ratios but with considerably large maximum and average lengths for paths (or for paths longer than certain thresholds) owing to the concentration disadvantage and connection advantage of scattered fractures. We comprehensively compare different 2D DFNs (including field-collected DFN, totally modeled DFNs, DFNs with field fracture size, and DFNs with field fracture locations) and conclude that generating statistically modeled DFNs with identical connectivity features is extremely difficult. Mechanical means that consider connections among fractures are recommended for DFN applications.

**Keywords** Discrete fracture network · Discrepancy · Statistical analysis · Natural fracture · Connectivity

## 1 Introduction

Discontinuities, including rock beddings, soft layers, structural fractures, and microfractures, act as distinctly weak parts and play primary roles in the deformational and mechanical characteristics of rock masses. As an important type of discontinuity, structural fractures are large in number and are stochastically distributed. Consequently, they pose a considerable challenge to engineering geologists when thoroughly exploring the influence of complicated and random fractures on mechanical weakening and deformation augmentation on rock masses. Therefore, structural fractures are extensively emphasized in geometric and mechanical rock mass analyses (Einstein et al. 1983; Chen et al. 1995; Hudson and Harrison 1997; Grenon and Hadjigeorgiou 2003;

✉ Shengyuan Song  
songshengyuan@jlu.edu.cn

✉ Peihua Xu  
xuph@jlu.edu.cn

<sup>1</sup> College of Construction Engineering, Jilin University, Changchun, Jilin 130026, China

<sup>2</sup> Department of Civil and Environmental Engineering, University of California Berkeley, Berkeley, CA 94701, USA

<sup>3</sup> China Water Northeastern Investigation, Design and Research Co., Ltd, Changchun, Jilin 130026, China

<sup>4</sup> North China Power Engineering Co., Ltd. of China Power Engineering Consulting Group, Changchun, Jilin 130000, China

<sup>5</sup> Liaoning Non-ferrous Geological Exploration Research Institute Co, Ltd, Shenyang, Liaoning 110013, China

Jing 2003; Sisavath et al. 2004; Esmaili et al. 2010; Vazaios et al. 2018).

In terms of current technologies, structural fractures inside rock masses are invisible. Therefore, only one-dimensional (1D) and two-dimensional (2D) traces of fractures on rock outcrops can be collected, and those in other 2D sections or in three-dimensional (3D) spaces are unavailable. Consequently, modeling methods of discrete fracture network (DFN), which is an ensemble of structural fractures and can be used to generate fractures in other sections or spaces, have achieved tremendous development in the recent 50 years (Chen et al. 1995; Xu and Dowd 2010; Thovert et al. 2011; Malinouskaya et al. 2014; Bonneau et al. 2016; Han et al. 2016; Fang et al. 2017). DFN modeling is primarily accomplished on the basis of stochastically geometric technologies. The geometric factors of DFN, such as trace length (or 3D disc size), orientation, density, and location, have been widely examined by engineering geologists (Priest and Hudson 1981; Kulatilake et al. 1984, 1990, 2011; White and Willis 2000; Thovert and Adler 2004; Chen et al. 2005; Thovert et al. 2014). Complicated considerations have been occasionally combined in DFN modeling, such as mechanical aspects (Davy et al. 2013; Lei et al. 2015; Li et al. 2018). To date, DFN modeling method is supposed to be relatively perfect in theory and has been widely used in practical rock engineering analysis (Grenon and Hadjigeorgiou 2003; Chen et al. 2005; Elmo et al. 2014; Bauer and Toth 2017; Vazaios et al. 2017; Zhang et al. 2017a).

Fractures generated by DFN modeling method are statistically representative of the field natural ones, with inconsistency in the specific location and corresponding geometric factors of a fracture. Discrepancy occurs between statistically modeled and field-collected DFNs (Esmaili et al. 2010; Zhang et al. 2013, 2017b). Some scholars have diminished the discrepancies by increasing the number of statistically modeled DFNs and subsequently taking their statistical results as references of rock mass structural analysis (Elmo et al. 2013; Stacey et al. 2015). Some researchers have argued that DFNs, which are entirely generated based on geometric statistics, may not be representative, and thus require additional mechanical considerations (Lei et al. 2015; Bonneau et al. 2016; Li et al. 2018). However, the generation technique of mechanical DFNs has been limited. Research has indicated the discrepancies that should be considered in DFN application. The following references, which are introduced as typical examples, directly focused on DFN discrepancies. Odling and Webman (1991) compared a natural fracture pattern with ten statistically modeled realizations. The permeability of the natural pattern was indicated to be increasingly underestimated with the increase in the permeability contrast between rock matrix and fractures. Afterwards, Odling (1992) found that the spatial distributions of natural and modeled DFNs significantly varied,

which led to distinctly different degrees of connectivity and fractal patterns. Belayneh et al. (2009) researched the permeability of outcrop-based deterministic analogs and several stochastic realizations. The hydraulic properties were proven to vary dramatically. Lei et al. (2015) examined the validity of statistically modeled DFNs in representing field-collected fractures in terms of their geomechanical and hydraulic responses. The results demonstrated that modeled DFNs were only representatives for fixed mechanical conditions, which might be unreliable if mechanical changes occurred.

Discrepancies between field-collected and statistically modeled DFNs play extremely crucial roles in determining the mechanical and deformational properties of rock mass, given that DFN is the fundamental procedure in rock mass analysis. However, discrepancy studies are inadequate to understand DFN application limitations. Well-known important problems explain the discrepancies occurring in terms of fracture locations and geometric factors, the manner in which discrepancies are quantitatively described, and the manner in which these discrepancies can be considered in DFN application. The current study takes sluice foundation rock mass in Datengxia Hydropower Station as an example to establish a comprehensive analysis of these problems. Its natural fractures are collected, and 20 2D DFNs are statistically modeled on the basis of stochastic theories (Sect. 2). Discrepancies in fracture position and trace length distributions are examined (Sect. 3). The discrepancies in 2D connectivity determined by depth-first search (DFS) algorithm are quantitatively described (Sect. 4), and discussion to these discrepancies is presented (Sects. 5, 6).

## 2 Study Area and Data Acquisition

### 2.1 Study Area

This study uses fractures developed in a sluice foundation rock mass in Datengxia Hydropower Station as the study object (Fig. 1a). The hydropower station is located at the Pearl River in Guiping City, China and has a main dam size of 80 m (height)  $\times$  1343 m (length) and a reservoir storage capacity of  $2.813 \times 10^9$  m<sup>3</sup>. Mainly designed for power generation, flood control, and shipping, this station has been set to be the primary engineering of China Ministry of Water Resources. The foundation of the sluice plays a crucial role in dam safety as a portion of the main stream due to its expected high hydrostatic pressure exerted by a 61 m upstream water level and a 22.7 m downstream water level (normal storage condition). Therefore, studying the characteristics of discontinuities developed inside the sluice foundation rock mass is essential.

The hillocks downstream the sluice are sliced off and cleaned out, thereby facilitating our discontinuity collection.

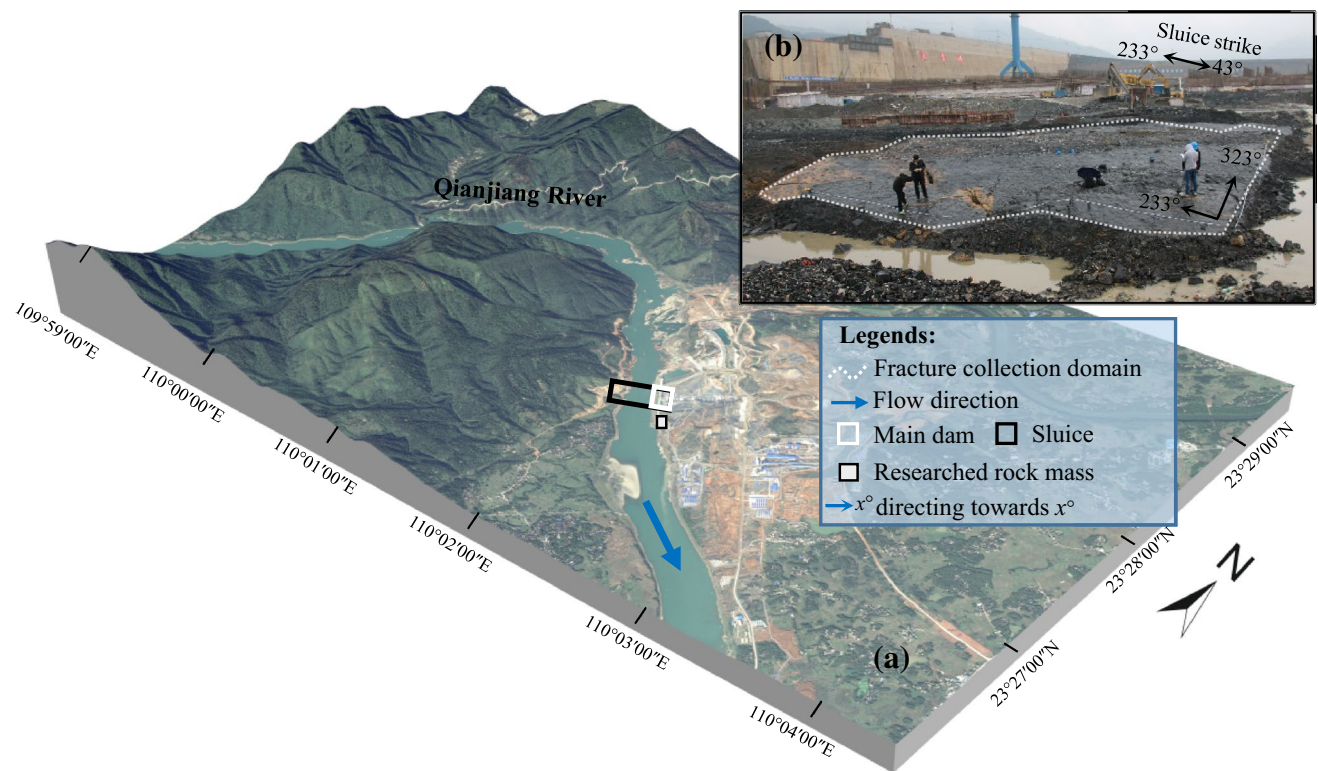


**Fig. 1** Study area and fracture-collection domain. **a** Location of the main dam and its sluice. **b** Domain of the collected fractures developed in the sluice foundation rock mass

The moist rock exposures indicate a shallow water level condition. This study selects a headmost cleaned portion; its location is illustrated in Fig. 1a, and the overall perspective is shown in Fig. 1b. This portion is covered by formations of Lower Devonian ( $D_1$ ) limestones, with bed thickness of more than 20 m and bedding surfaces dipping at the directions of  $100^\circ$ – $110^\circ$  with dip angles of  $10^\circ$ – $15^\circ$ .

Although a few faults are developed around the sluice, their scales are relatively small. Moreover, their strikes are nearly the same as the direction of the hydrostatic pressure. Therefore, the influences of the faults on the safety of the sluice dam are considerably reduced. This study focuses on stochastically distributed structural fractures, which are believed to have a substantial effect on sluice safety. Collection and details of the fractures are introduced in Sect. 2.2.

## 2.2 Collection of Field Fractures

Sampling window method (Kulatilake and Wu 1984) is applied to collect the fractures in the cleaned rock exposure, as exhibited in Fig. 1b. Fractures, with trace lengths shorter than 0.3 m, are truncated during the collection. The geometric characteristics, including the start and end coordinates, orientation (dip direction and dip angle), aperture

width, filling, moisture, weathering degree, and surface morphology of fractures with trace lengths larger than 0.3 m, are recorded. A total of 667 fractures are eventually detected, and their traces are shown in Fig. 2.

An overwhelming majority of fractures are steeply dipped with angles larger than  $70^\circ$  and embody shear mechanism with straight traces. The field observation indicates that the fracture traces predominantly extend along two directions, with one direction similar to and the other one perpendicular to the sluice strike ( $233^\circ$  or  $43^\circ$ ). Therefore, two sets are categorized using the method suggested by Chen et al. (1995), and their average orientation results (dip toward  $296^\circ$  and  $210^\circ$ ) are approximately consistent with our field judgment (Table 1 and Fig. 3). This fracture set categorization aids mechanical analysis, because the hydrostatic pressure is similar to or perpendicular to the mean fracture strikes.

Trace lengths of the aforementioned two fracture sets are examined, showing that they follow log-normal distribution (Table 1), as elucidated in Sect. 2.3. P20 (fracture number per area,  $1/m^2$ ) and P21 (total fracture trace length per area,  $m/m^2$ ) are derived to depict the 2D fracture density (Table 1).

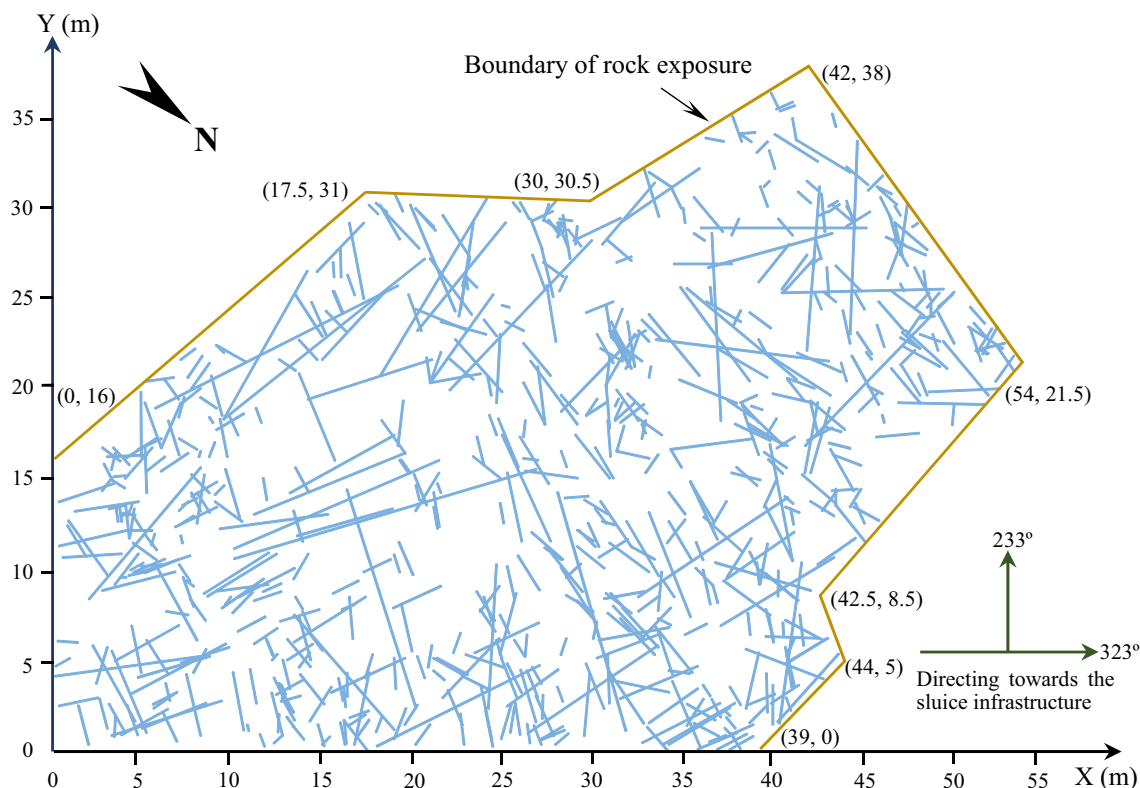


**Fig. 2** Traces of the fractures collected on the rock exposure of the sluice foundation rock mass

**Table 1** Information on the traces of fractures collected in the sluice foundation rock mass

Fracture set	Fracture number	Fracture orientation		Fracture trace length			Fracture density	
		Dip direction (°)	Dip angle (°)	Mean (m)	Standard deviation (m <sup>2</sup> )	Distribution type	P20 (1/m <sup>2</sup> )	P21 (m/m <sup>3</sup> )
1	466	296	80	2.14	1.89	Log-normal	0.34	0.72
2	201	210	82	2.61	2.68	Log-normal	0.14	0.38

### 2.3 Generation of Statistically Modeled DFNs

2D DFN modeling method, which has been extensively used in rock mass analysis, is used to regenerate fractures on the rock exposure with the reason, as introduced in Sect. 3. The manner in which the elements for DFN generation is determined is described as follows.

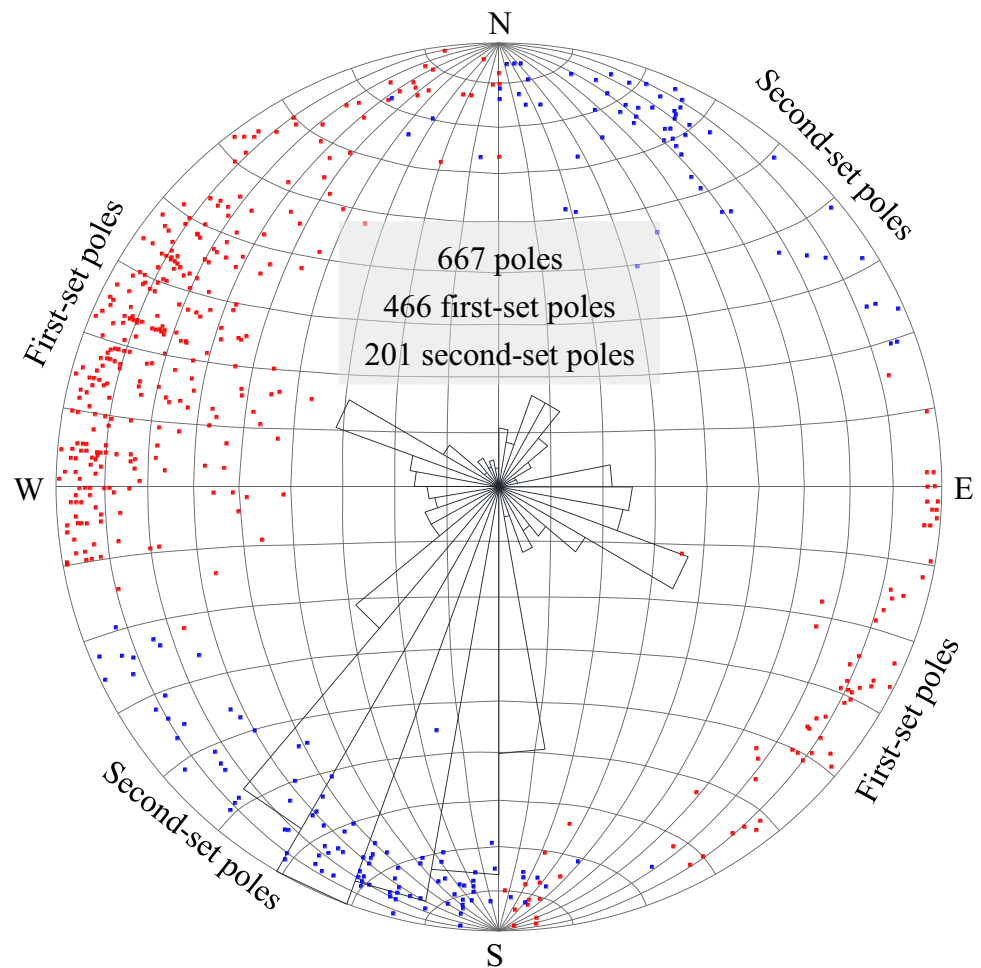
The collected fractures are located within a polygonal region with an area of 1390 m<sup>2</sup> (Fig. 2). Generating fractures within this irregular region is definitely inconvenient; thus, a slightly larger region with a size of 60 m (X axis) × 40 m (Y axis) is selected as the modeling region to accommodate the generated fractures.

A total of 466 and 201 field fractures of sets 1 and 2 are collected, respectively, and their densities are calculated (Table 1). The fracture numbers in the 60 × 40 m region can

be redetermined by augmenting 2400/1390 times. Consequently, this process results in 805 and 346 fractures that can be simulated for sets 1 and 2, respectively. The two fracture numbers are ultimately applied to represent the simulated fracture density and generate the fractures in the modeling region.

Fracture positions are always considered to follow a homogeneous (Poisson) model, a nonhomogeneous process, a cluster process, or a Cox process (Lee et al. 1990; Xu and Dowd 2010). Among the four considerations, homogeneous (Poisson) model is mostly used in DFN generation (Chen et al. 1995; Bonneau et al. 2016; Zhang et al. 2017b). In addition, the researched rock masses belong to the same lithology with identical physical and mechanical characteristics. Thus, the mostly used Poisson model is applied in this study, and the discrepancy analysis is performed

**Fig. 3** Poles and strike rose diagrams of the 667 collected fractures. Red poles represent the first-set fractures and blue poles represent the second-set fractures (color figure online)



on the basis of this model. In this study, the midpoint of a fracture trace is used to represent the fracture position. The midpoints of the aforementioned 805 and 346 fractures are uniformly distributed in the  $60 \times 40$  m region. Notably, the spatial organization of field-collected fractures differs from the homogeneous point process results according to two-point correlation dimension (Bonnet et al. 2001; Bonneau et al. 2016). Section 6 further discusses this finding. Considering the common use of Poisson model in DFN generation especially in rock masses with identical mechanical and deformational features as our study object, the discrepancy analysis is continuously carried out on the basis of the Poisson model (Sects. 4.2, 5.1). In addition, the discrepancy is executed on the basis of the field fracture point organization reflecting the field fracture location organization as the supplementary verification (Sect. 5.2).

The fracture trace length is an extremely crucial element that influences the rock mass characteristics. Therefore, this element is widely researched by scholars worldwide (Priest and Hudson 1981; Kulatilake and Wu 1984; White and White 2000; Wu et al. 2011). A plausible method for generating fracture traces in a statistical homogenous domain is

to examine the probability distribution of the trace lengths of field-collected fractures and to apply this distribution to model the trace length population. Chi-square and Kolmogorov–Smirnov (KS) goodness-of-fit tests are common and acceptable methods to determine the probability distribution of the trace length data. The two tests show that log-normal distribution is optimal to describe the trace lengths of field-collected fractures, which thoroughly introduced in Sect. 3.1. Therefore, log-normal distribution and its statistical parameters (Table 2) are applied for trace length generation. Subsequently, 805 and 346 trace lengths following log-normal distributions, with corresponding location and scale parameters listed in Table 2, are generated for fracture sets 1 and 2, respectively.

Fracture orientations are typically scattered and bivariate, which pose a complicated problem to rock mass analysis. These orientations are frequently assumed to follow bivariate Fisher, normal, Bingham, or experimental distribution (Kulatilake et al. 1990; Jayaram and Baker 2008; Liu et al. 2018). The current study applies the experimental distribution, as indicated in Fig. 4. The fracture orientations are projected in the equal-area Schmidt (Fig. 3) and

**Table 2** Density function parameters and statistics determined by Chi-square and KS goodness-of-fit tests

Distribution type	Set 1					Set 2				
	Density function parameters			$\chi^2$	$D_n$	Density function parameters			$\chi^2$	$D_n$
	A	B	C			A	B	C		
Triangle	0.50	4.20	1.72	534	0.46	0.50	4.60	1.32	325	0.47
Uniform	0.50	12.72	–	1137	0.61	0.50	17.50	–	641	0.63
Poisson	2.14	–	–	1317	0.36	2.61	–	–	712	0.50
Normal	2.14	1.89	–	2341	0.34	2.61	2.68	–	1123	0.38
Exponential	0.47	–	–	76	0.13	0.38	–	–	30	0.11
Log-normal	0.48	0.76	–	29	0.04	0.59	0.85	–	17	0.05
Gamma	1.28	1.67	–	69	0.15	0.94	2.77	–	29	0.17

A, B, and C of Triangle distribution represent lower limit, upper limit, and mode, respectively; A and B of Uniform distribution represent lower and upper limits, respectively; A of Poisson distribution represents the rate parameter equal to sample's average value; A and B of normal distribution represent average and standard deviation values, respectively; A of Exponential distribution represents the rate parameter equal to the reciprocal of average value; A and B of the Log-normal distribution represent the location and scale parameters, respectively; A and B of Gamma distribution represent shape and rate parameters, respectively

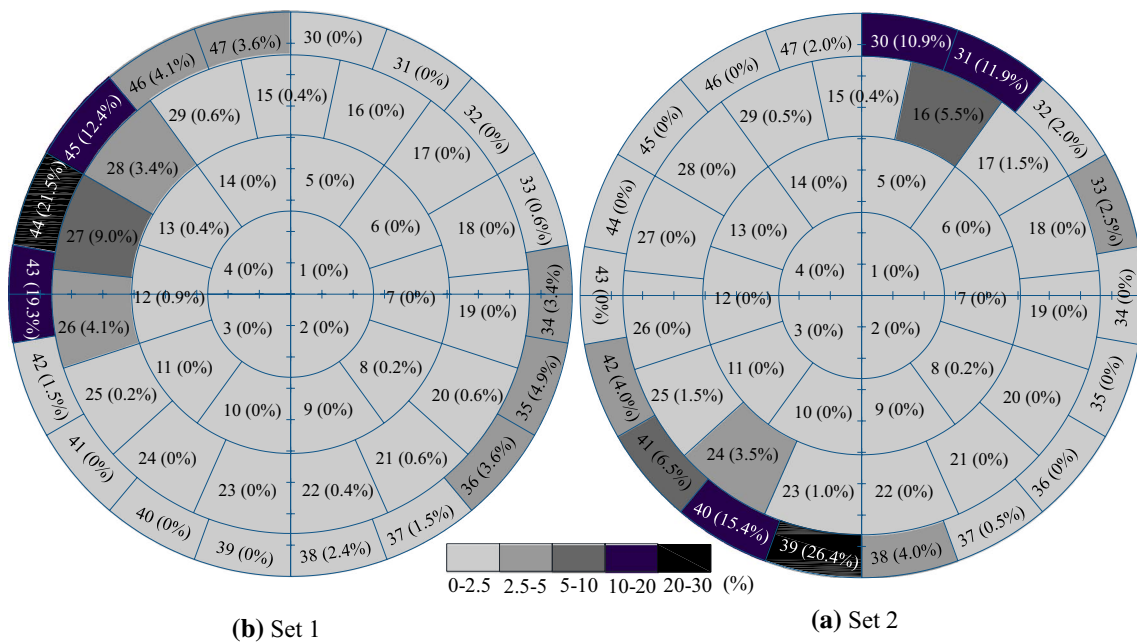


**Fig. 4** Equal-area Schmidt projection diagram of the collected fractures.  $x$  ( $y\%$ ) represents the ratio ( $y\%$ ) of fracture number in the  $x$ th patch to the total fracture number

divided into 47 patches, with each showing its fracture number ratio. The modeled fracture orientations follow these number ratios. Orientations (dip and dip angle) in each patch follow uniform distribution, which can greatly simplify the generation of fracture orientations. The fractures in the modeled 2D DFN are only characterized by extension directions, which are equal to the fracture plane strikes for the horizontal rock outcrop. Therefore, strikes of modeled fractures are used to represent the 2D fracture orientations (extension direction).

The aforementioned steps determine the fracture accommodation scope, density (number), position, trace length, and extension direction. A Monte Carlo simulation can be used to stochastically synthesize the latter three geometric factors to generate 805 and 346 fractures for sets 1 and 2 in the  $60 \times 40$  m region, respectively (Chen et al. 1995). Countless DFNs can then be generated (Esmaili et al. 2010; Zhang et al. 2013; Vazaios et al. 2018), based on which fractures inside the polygonal field-collection region (Fig. 2) can be determined. Geometric parameters of some

DFNs inside the region inevitably deviate from those of the collected fractures. Therefore, we select eligible DFNs with acceptable deviations. The number ( $n$ ) of fracture and the parameters of fracture length trace log-normal distribution law (average  $\mu$ , standard deviation  $\sigma$ ) collected on the field (Table 1) are adopted to evaluate the validity of modeled DFNs. DFNs with fracture numbers within  $n \pm 10$  and trace length parameters within  $\mu \pm 0.1$  (m) and  $\sigma \pm 0.1$  (m) are selected as eligible ones and applied for the following simulations.  $n$  should eliminate fractures smaller than 0.3 m, which corresponds to the operation of field-collected fractures (Sect. 2.2).

A large amount of DFNs that meet the aforementioned requirements can be determined in the field-collection region. This study illustrates three modeled DFNs as examples in Fig. 5, from which the distributions of fractures in different DFNs noticeably vary. Therefore, DFN variability should be the focus, that is, only the stochastic evaluations of DFNs draw rational results. Eventually, this study later uses 20 modeled DFNs for the discrepancy analyses.

### 3 Discrepancy in Fracture Geometric Parameters

DFN technology can be used in both 2D (linear fracture traces) and 3D (planar fractures) modeling methods. These models are helpful in evaluating the mechanical and deformational characteristics of rock masses (Baghbanan and Jing 2008; Zhang et al. 2017b; Li et al. 2018). This study carries out discrepancy analysis between field-collected and statistically modeled DFNs. Although 3D analysis is valuable, collecting 3D fractures in field is impractical for today's technologies. Thus, conducting 3D discrepancy analysis is difficult or even impossible. Given that only field-collected 2D traces are actual and thus can be used for

practical discrepancy analysis, 2D DFNs corresponding to field-collected fracture parameters are modeled.

We use experimental distribution to generate orientations of modeled fractures to ensure that the modeled orientations are close to the field data (Fig. 4). Fracture density is considered to determine the fracture number, which is made to fit the field fractures. Density is not the discrepancy research focus. Distribution of fracture trace lengths and regular pattern of fracture locations (positions) are highlighted, considering the aforementioned geometric characteristics of the fractures.

#### 3.1 Trace Length Distribution

Size is the most influential element in the geometric characteristics of fractures. Therefore, the fracture trace length is extensively examined, among which the trace length distribution is one of the most important research points (Priest and Hudson 1981; Kulatilake and Wu 1984; White and White 2000; Wu et al. 2011). Two interesting arguments are worth elaborating. First, can trace lengths of naturally developed fractures be perfectly described by a theoretical probability distribution? Differences inevitably exist between the practical distribution of field-collected fracture trace lengths and the theoretical distribution, which require quantification and qualification for rock mass analyses. Second, can a single probability distribution perfectly describe trace lengths of field fractures? To investigate these questions, we compare the frequencies of field-collected trace length probability distribution with those of the theoretical distribution confirmed by Chi-square and KS goodness-of-fit tests.

Chi-square and KS goodness-of-fit tests are plausible methods to determine which probability distribution the observation (field-collected fracture trace lengths) follows by comparing the observation sample with designed probability distributions (Zhang et al. 2013; Song et al. 2017). The difference between the two tests is that the former

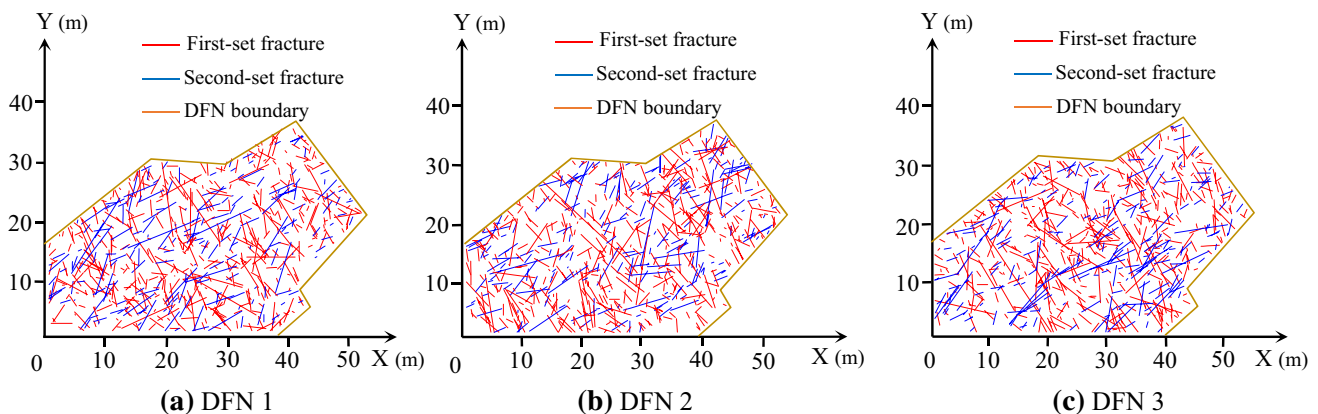


Fig. 5 Three examples DFNs in the fracture-collection region with acceptable values of  $n$ ,  $\mu$ , and  $\sigma$

compares the cumulative difference of probability density function (PDF), whereas the latter compares the maximum difference of cumulative distribution function (CDF). The statistics of Chi-square ( $\chi^2$ ) and KS tests ( $D_n$ ) are exhibited by Eqs. (1) and (2), respectively:

$$\chi^2 = N \sum_{i=1}^n \frac{\left(\frac{O_i}{N} - p_i\right)^2}{p_i}, \tag{1}$$

where  $N$  is the total number of observations (field-collected fractures),  $n$  is the number of compared parts (i.e., the entire extension of the fracture trace lengths is divided into  $n$  parts, and each part is compared with its corresponding part derived from the designed PDF),  $O_i$  is the number of observation in the  $i$ th part, and  $p_i$  is the fraction of the  $i$ th part in the population of the designed PDF ( $Np_i$  is the theoretical count of the  $i$ th part):

$$D_n = \sup_x |F_n(x) - F(x)|, \tag{2}$$

where  $\sup_x$  is the supremum function,  $F_n(x)$  and  $F(x)$  are the empirical distribution function of the sample (field-collected fractures) and the CDF, respectively, and  $n$  is the number of compared parts, which is similar to that in Eq. (1).

Seven frequently used probability distributions (i.e., triangle, uniform, Poisson, normal, exponential, log-normal, and gamma distributions) are considered designed probability distributions in this study.  $\chi^2$  and  $D_n$  shown in Eq. (1) and (2) are calculated for each aforementioned distribution. The designed probability distribution with the minimum  $\chi^2$  or  $D_n$  values is considered the most suitable, and its PDF parameters are used for trace length generation mentioned in Sect. 2.3. Here, the comparison between calculated and critical test statistics, which requires determinations of degree of freedom and significance level, is weakened. Given the continuing controversy in the determination of key parameters such as significance level for critical test statistic, we emphasize the minimum test statistic judgement which can offer us the optimal probability distribution. Table 2 shows the test statistics of differently designed probability

distributions, with  $n = 12$ . As mentioned in Sect. 2.3, the log-normal distribution, which embodies the minimum test statistics, is selected.

Table 3 shows the Chi-square and KS goodness-of-fit test results under different compared parts  $n$ . The Chi square goodness-of-fit test of trace lengths of fracture 2 is taken as an example. The values of  $\chi^2$  are smaller than their critical ones when  $n = 12, 14,$  and  $16$  (significance level is 0.05), whereas, values of  $\chi^2$  are larger when  $n$  equals 8, 10, and 20. Therefore, the discrepancy between trace lengths of field-collected fractures and their theoretical PDF or CDF is proven to be variable.

Figure 6 exhibits the discrepancy under different values of  $n$ . The discrepancy (percentage difference) is small when the trace length is smaller than 5 m for fracture sets 1 and 2. Majority of the percentage difference values are smaller than 25%, whereas the values increase when the length is larger than 5 m, with most of them larger than 50%. Specifically, the theoretical values are larger than those of the field-collected fracture traces for lengths approximately ranging from 5 to 8 m, whereas the theoretical values are smaller for lengths larger than 8 m. The difference in fracture trace lengths results in discrepancies in rock mass characteristics, especially when the lengths are large; hence, this difference requires consideration.

In sum, the trace lengths of field-collected fractures in the sluice foundation rock mass in Datengxia Hydropower Station can be statistically described by a theoretical PDF. However, the discrepancies between the practical and theoretical PDFs should be considered. Section 5.2 will further describe the influence of this discrepancy on fracture connectivity. In addition, the field-collected fractures can be described by a single probability distribution. However, complicated situations may occur, as introduced in Sect. 6.

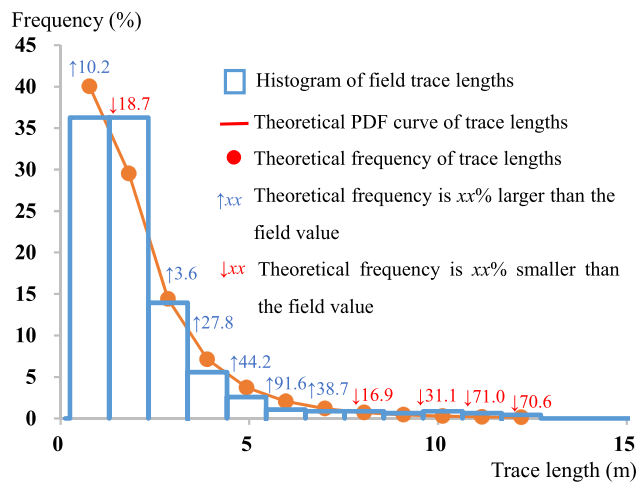
### 3.2 Regular Pattern of Fracture Location

As introduced in Sect. 2.3, fracture location is assumed to follow a homogeneous (Poisson) model; that is, fractures are stochastically distributed in rock masses. This handling

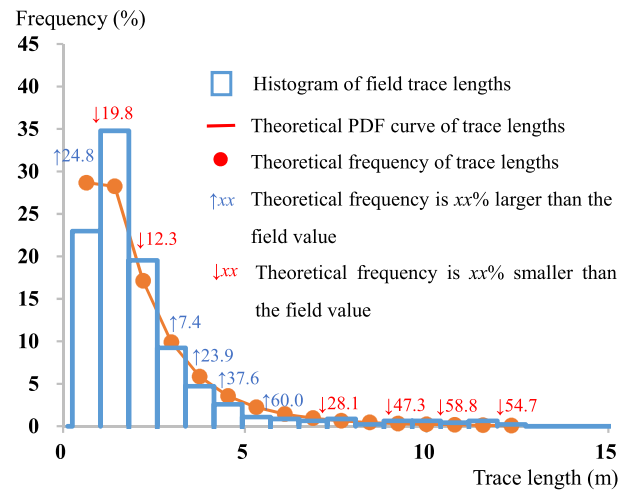
**Table 3** Chi-square and KS goodness-of-fit test results under different numbers of compare parts  $n$

Goodness-of-fit tests	Test results											
	Set 1						Set 2					
$n$	8	10	12	14	16	20	8	10	12	14	16	20
Chi square												
$N_f$	5	7	9	11	13	17	5	7	9	11	13	17
$\chi^2$	21.43	35.04	29.21	33.03	40.06	49.63	12.1	15.02	16.91	15.38	22.16	31.26
KS												
$N_f$	8	10	12	14	16	20	8	10	12	14	16	20
$D_n$	0.02	0.041	0.038	0.044	0.057	0.071	0.027	0.032	0.05	0.019	0.024	0.06

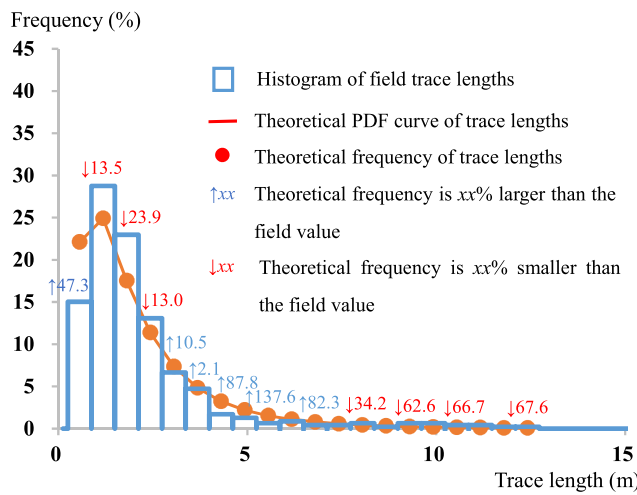




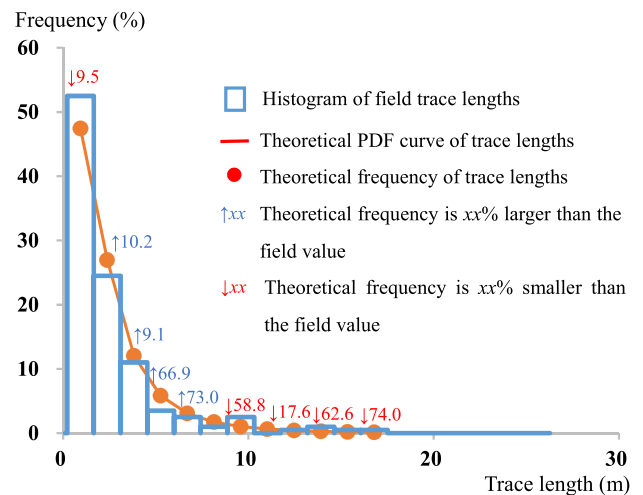
(a)  $n=12$  for fracture set 1



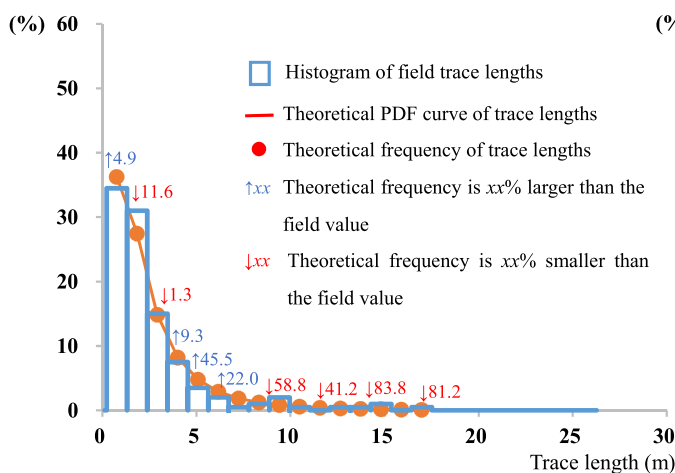
(b)  $n=16$  for fracture set 1



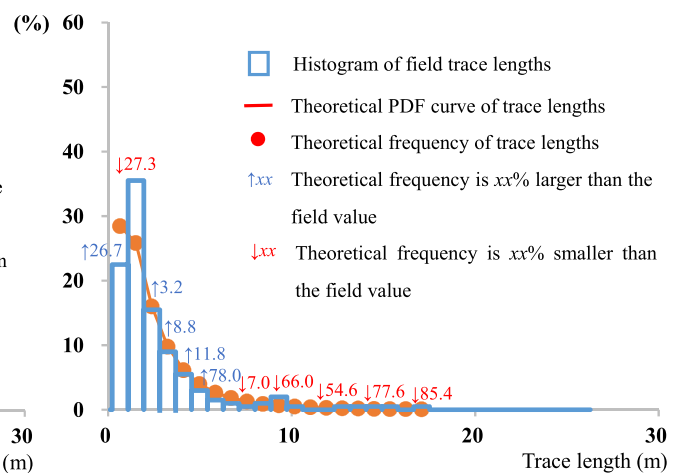
(c)  $n=20$  for fracture set 1



(d)  $n=12$  for fracture set 2



(e)  $n=16$  for fracture set 2



(f)  $n=20$  for fracture set 2

Fig. 6 Histograms and corresponding statistical curves in different comparison part number  $n$

pattern of DFN generation is widely accepted and used. However, this pattern is sometimes controversial (Davy et al. 2013); thus, the discrepancy between the natural and Poisson-modeled fracture locations must be explored. Accordingly, we propose a new variable called minimum spacing sequence (MSS) to assess the regular pattern of fracture locations. The  $i$ th element of MSS is determined by the minimum spacing between the  $i$ th fracture midpoint (representing the location) and the others. The number of the sequence is equal to that of the researched fractures.

MSS for the field-collected fractures is shown in Fig. 7a. For comparison, the MSS for Poisson-modeled fractures is shown in Fig. 7b–e, with Fig. 7c–e representing the first exemplified three DFNs exhibited in Figs. 5 and 7b representing the population of the 20 modeled DFNs. Discrepancies in MSS PDFs for field-collected and Poisson-modeled fractures are noticeable. The MSS PDF curves of Poisson-modeled fractures are approximately eudipleural with the right part slightly longer, whereas the curve of field-collected

fractures noticeably leans to the left. Therefore, quantitative examination of the difference is essential. This study applies the statistical measures (i.e., average, standard deviation, skewness, and excess kurtosis), and their values are presented in Fig. 8. Average, standard deviation, skewness, and excess kurtosis of MSS for field-collected fractures are 0.65 m, 0.44 m<sup>2</sup>, 1.52, and 4.19, respectively (Fig. 7a). They have a slightly smaller average and a slightly larger standard deviation but considerably larger skewness and excess kurtosis than the modeled fractures (Fig. 8).

Several outcomes can be summarized considering the results of the statistical measures. A small average of field-collected fractures implies that the MSS has small values. This finding indicates that the field-collected fractures are more concentrated to one another compared with the Poisson-modeled ones. By contrast, a large standard deviation indicates scattered locations. In sum, field-collected DFN has more small-spaced (concentrated) but do not lack large-spaced (scattered) fractures, which is contrary to the

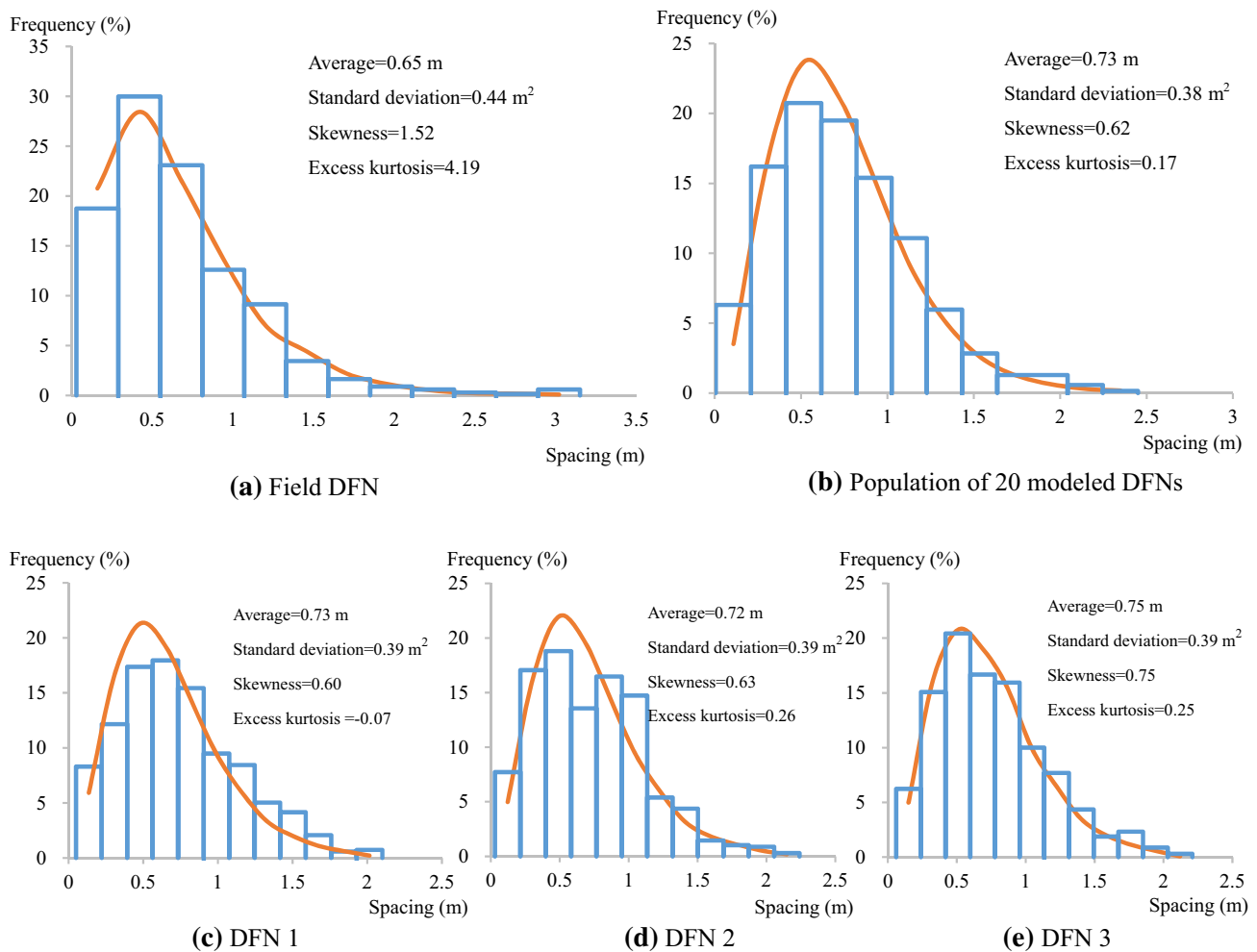
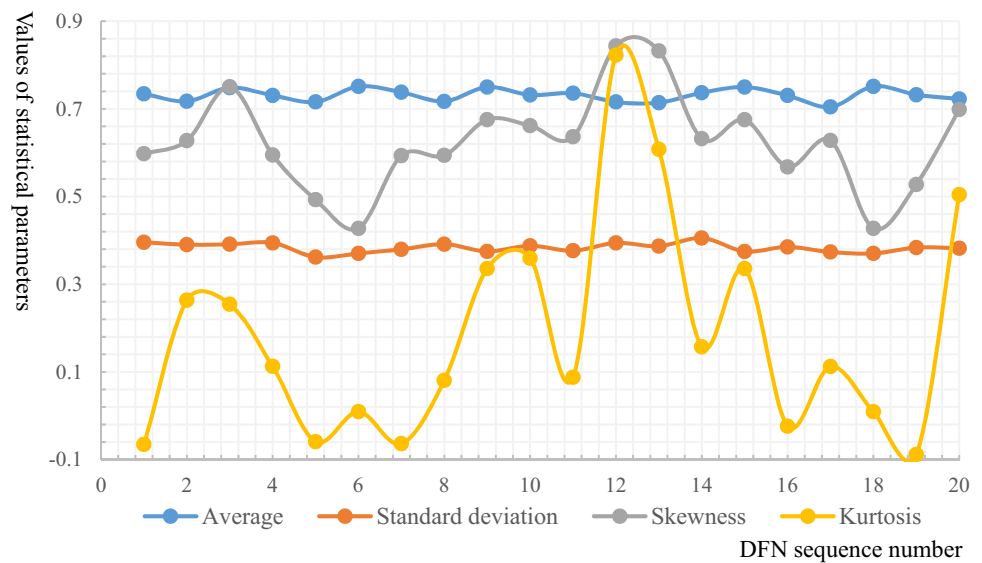


**Fig. 7** Minimum spacing series (MSS) for field-collected and statistically modeled DFNs

**Fig. 8** Statistical parameters of 20 statistically modeled DFNs



conception that fractures are uniformly distributed. Skewness and excess kurtosis have noticeable powers to embody differences between field-collected and Poisson-modeled MSS DFNs. The skewness value for the field-collected fractures is 1.52, which is considerably larger than those for either the 20 modeled fractures (ranging from 0.43 to 0.87) or for their population (0.62). This result indicates that the MSS PDF curves for field-collected and Poisson-modeled fractures are all positively skewed (left-leaning curved), with the curve for the field-collected fractures having a considerably longer and thinner right tail. Therefore, the MSS values for field-collected fractures have remarkably more minimum spacing values; that is, field-collected fractures are more concentrated than the Poisson-modeled fractures. The excess kurtosis value (kurtosis value minus 3) for the field-collected fractures is 4.19, which is markedly larger than those for either the 20 modeled fractures (ranging from  $-0.09$  to 0.82) or for their population (0.17). This result indicates that the MSS PDF curves for the Poisson-modeled fractures have approximately the same or slightly more extreme outliers than that of the normal distribution curve (excess kurtosis equal to 0); by contrast, the MSS PDF curve for the field-collected fractures is typically leptokurtic, which have much more extreme outliers.

In sum, the field-collected fractures are concentrated to one another and have extensive minimum spacing values. Consequently, the MSS PDF curve for the field-collected fractures leans to the left and has a large extension with a long and thin right tail.

## 4 Connectivity Analyses of Field-Collected and Modeled DFNs

Differences in trace length and location distributions between the field-collected and statistically modeled DFNs evidently exist in Sect. 3. Whether these differences will result in discrepancy in rock mass characteristics requires assessment. Fracture connectivity, which emphasizes the connections of fractures, is widely used in assessing the hydraulic diffusivity of a rock mass formation (Hao et al. 2008; Adler et al. 2012; Bonneau et al. 2016; Li et al. 2018). Connections of fractures, which comprehensively depend on fracture geometric characteristics, indicate the deformational and mechanical properties of rock masses (Yang et al. 2018). Therefore, fracture connectivity is applied to examine the discrepancy in rock mass characteristics.

### 4.1 DFS Algorithm

Discontinuities, especially structural fractures, are large in number and are stochastically distributed inside the analyzed rock masses. Summarizing fracture connection disciplines is time-consuming. This work uses the DFS, which is an efficient algorithm widely used for searching connected tree or graph data structures, to quantify the fracture connectivity.

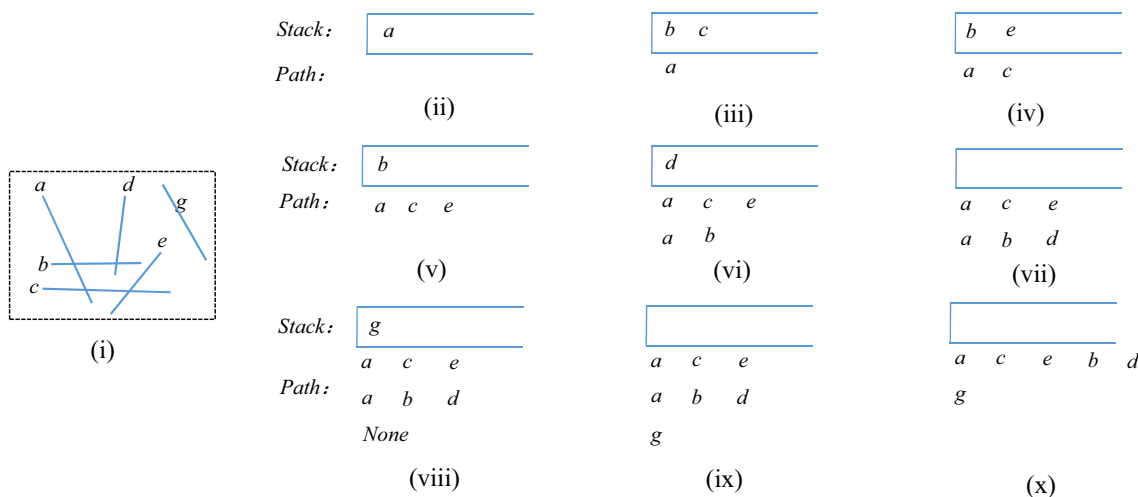


**Fig. 9** Procedures of DFS algorithm for a simple DFN. Stack accommodates fractures in (i); path represents connected fractures taken out of the stack. Steps from (ii) to (v) show forward searches of path a-c-

e; steps from (vi) to (vii) show backward and traverse searches of path a-b-d; steps from (viii) to (ix) show a new search of path g; and step (x) shows the merging of paths having common fractures

DFS was first proposed to solve a maze problem (Bondy and Murty 2010) that somewhat resembles the connected path searching of our study. The present work uses an illustrational DFN shown in Fig. 9i determine the fracture connectivity through the following procedures, which are implemented using stacks: (1) arbitrarily selecting a fracture from the DFN and placing its connected fractures into the stack; (2) taking the last fracture inside the stack out and placing its connected and unsearched fractures into the stack; (3) moving backwards to find fractures to traverse if no fracture is in the stack; and (4) starting new research and repeating the abovementioned procedures until all the fractures are searched.

Using the abovementioned procedures shown in Fig. 9ii-ix, connectivity paths can be searched as Fig. 9x. Further specific procedures can be referred to Bondy and Murty (2010), which are not introduced in detail here.

### 4.2 Results

Connectivity characteristics, such as the number of connected fractures and the length of a path (sum of connected fracture lengths), can be confirmed using the DFS algorithm, as shown in Sect. 4.1. Searching of the field-collected and the first three DFNs, as shown in Figs. 2 and 5 are taken as examples. The results are presented in Fig. 10, which show single fracture paths (carmine marked), clustered fracture paths (light green marked) that comprise connected fractures, and the longest path (black marked).

Specifically, searching of the field-collected fractures results in 62 clustered fracture paths, 200 single fracture paths, and 3 longest paths, with lengths sufficiently close and all larger than 130 m (Fig. 10a). We mark the number of

clustered and single fracture paths as  $N_1$  and  $N_2$ , respectively, and the length and fracture number of the longest path as  $L$  and  $n$ , respectively. These parameters are listed for the first three statistically modeled DFNs, as shown in Fig. 10b-d. The results show that the modeled DFNs possess small  $N_1$ , large  $N_2$ , and extremely large  $n$  and  $L$ .

We primarily account for the connectivity discrepancies given the following reasons. Fracture locations of statistically modeled DFNs follow the Poisson model, which is different from the field-collected fractures that are more concentrated to one another (Sect. 3.2). Consequently, the modeled fractures have a low degree of concentration, featured by small  $N_1$  values. Moreover, scattered fractures for modeled DFNs easily result in single fractures (large  $N_2$ ), which are not linked with other fractures. From another view, the scattering feature increases the opportunity for a fracture to connect with one another in a varying location; thus, statistically modeled DFNs have considerably large  $n$  and  $L$  values.

This section only samples three statistically modeled DFNs, and other modeled DFNs' results and specific corresponding comparison can be found in Sect. 5.

## 5 Discrepancy in Connectivity Analysis Results

Section 4.2 preliminarily compares the path numbers and lengths of field-collected fractures with those of the three statistically modeled DFNs, which is inadequate for examining discrepancies. This section extends the comparison to all of the 20 modeled DFNs and to other specific connectivity analysis results.

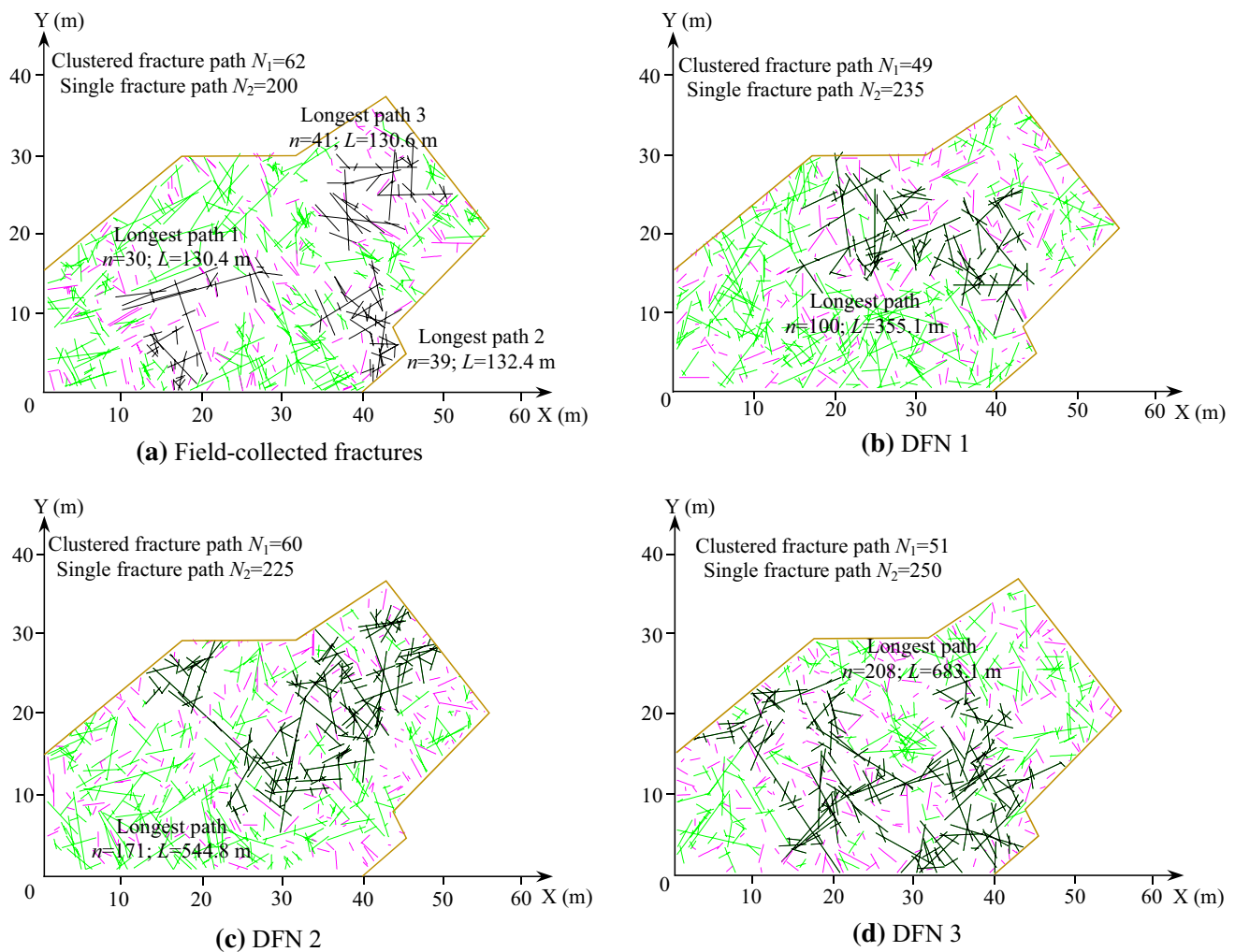


**Fig. 10** DFS results for field-collected and the first three statistically modeled DFNs. Single paths are marked by carmine fractures, clustered paths are marked by light green fractures, and the longest path is marked by black fractures (color figure online)

## 5.1 Discrepancies in Path Number and Length

Comparisons shown in Fig. 10 are extended to all of the 20 statistically modeled DFNs. The results are shown in Fig. 11a, with exhibited regular patterns corresponding to those elaborated in Sect. 4.2. That is, the statistically modeled DFNs possess small  $N_1$ , large  $N_2$ , and considerably large  $n$  and  $L$ . Notably, the  $N_2$  and total path number  $N$  (equal to  $N_1 + N_2$ ) of modeled DFNs are approximately 10–40 more than those of the field-collected fractures. However, this difference is unapparent when drawn in Fig. 11a.

A large proportion of paths are characterized by single fracture ones, with clustered fracture paths only accounting for 12–24% of all the paths. We use  $CR$  to represent the ratio of the clustered fracture paths to the total paths (Fig. 11a).  $CR$  values of statistically modeled DFNs (ranging from 12 to 23%) are all smaller than that of the field-collected fractures (24%). This conclusion verifies that the

field-collected fractures tend to concentrate to one another and consequently have a large  $CR$  value.

Longer paths have more influence on rock mass properties than shorter ones. Accordingly, we study paths longer than certain thresholds. This work sets thresholds to 10, 20, 30, 40, and 50 m, with the total lengths for paths longer than these thresholds marked as  $TL_{10}$ ,  $TL_{20}$ ,  $TL_{30}$ ,  $TL_{40}$ , and  $TL_{50}$ , respectively. The results are shown in Fig. 11b, which indicates that  $TL_{10}$ – $TL_{50}$  of statistically modeled DFNs distribute around the corresponding values of the field-collected fractures. The  $TL_{10}$ – $TL_{50}$  for field-collected and modeled DFNs are statistically the same. When considering the average of the field-collected and all the 20 statistically modeled DFNs,  $TL_{10}$ ,  $TL_{20}$ ,  $TL_{30}$ ,  $TL_{40}$ , and  $TL_{50}$  account for 69.7%, 63.5%, 60.1%, 56.5%, and 54.7% of the total path lengths (sums of all fracture lengths), respectively. The single longest path length accounts for 41.8% of the total length. Therefore, emphasis on few

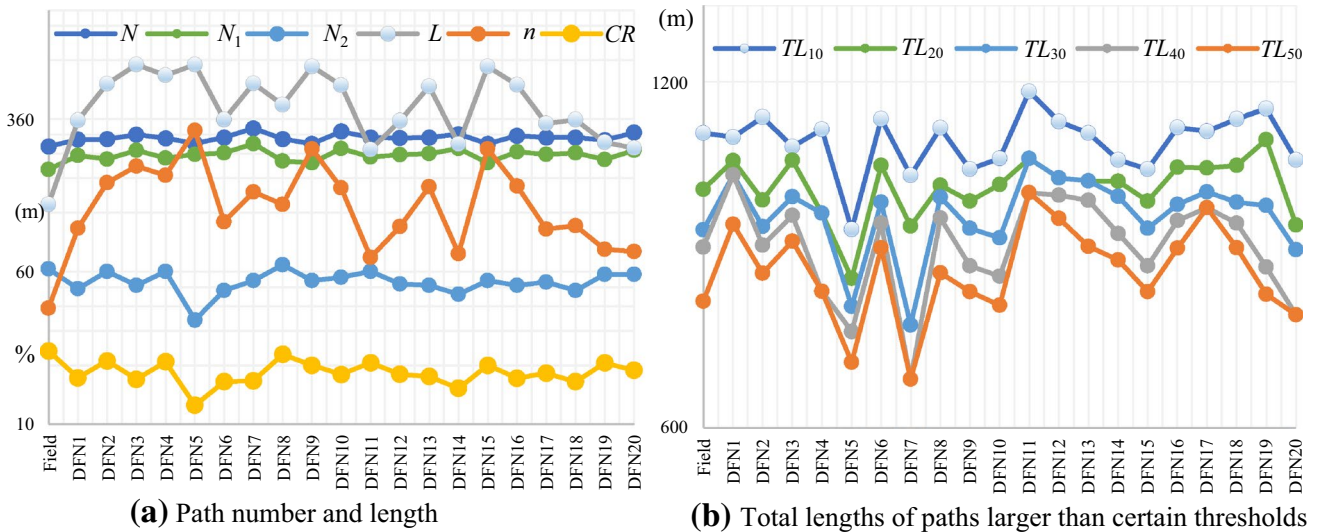


**Fig. 11** Numbers and lengths of searched paths.  $N$ ,  $N_1$ , and  $N_2$  are numbers of total paths, single fracture paths, and clustered fracture paths, respectively;  $L$  is the length of the longest connected path and

$n$  is this path's fracture number;  $CR$  is the ratio of the clustered fracture paths to total paths;  $TL_x$  is total length for path longer than  $x$  m

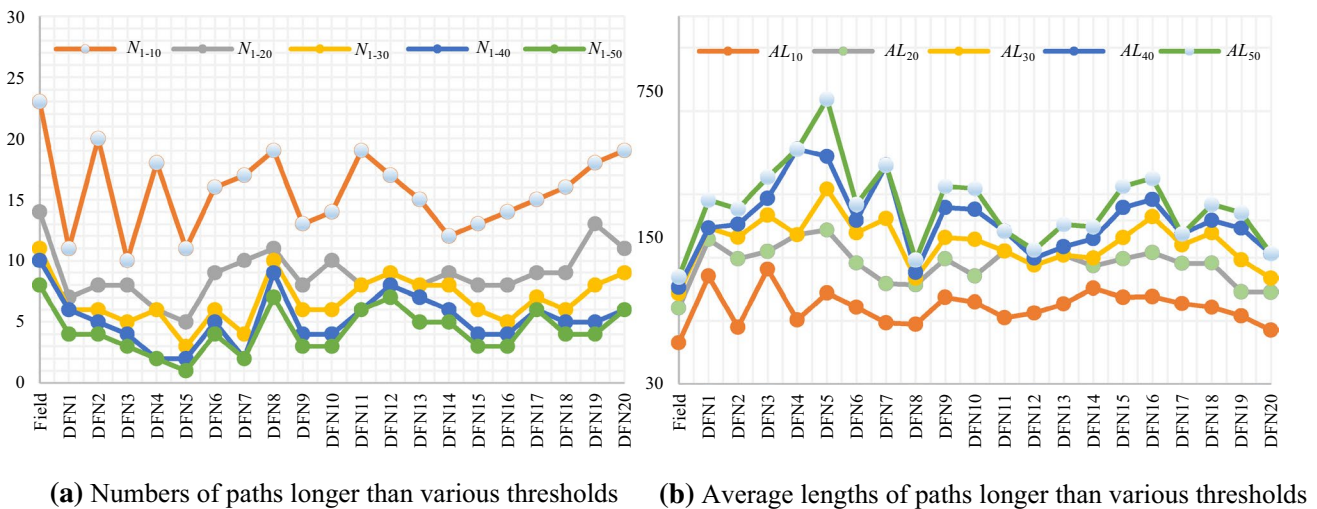


**Fig. 12** Numbers and average lengths of paths longer than various thresholds for field-collected and statistically modeled DFNs.  $N_{1-x}$  and  $AL_x$  are number and average length of paths longer than  $x$  m

but significant large-scale paths can simplify rock mass analyses.

Subsequently, we count the numbers of path longer than the aforementioned thresholds, which are marked as  $N_{1-10}$ ,  $N_{1-20}$ ,  $N_{1-30}$ ,  $N_{1-40}$ , and  $N_{1-50}$ . As shown in Fig. 12a,  $N_{1-10}$ – $N_{1-50}$  for the statistically modeled DFNs are all smaller than their corresponding values of the field-collected fractures. This result indicates that average lengths (marked as  $AL_{10}$ ,  $AL_{20}$ ,  $AL_{30}$ ,  $AL_{40}$ , and  $AL_{50}$ ) become larger or considerably larger (Fig. 12b). This tendency is similar to the results derived from Figs. 10 and 11. We

ascribe this phenomenon to the scattering features of the statistically modeled DFNs, as explained in Sect. 4.2.

The statistically modeled DFNs can scarcely represent the field-collected fractures. However, DFN modeling remains in use as an efficient method for rock mass analyses. The problem exposed to us is how we can use DFN while comprehensively considering the discrepancies in path properties between field-collected and statistically modeled DFNs. Fracture connectivity properties require consideration, similar to the those of the conventional geometric characteristics (e.g., fracture orientation, size, and density) when selecting

eligible DFNs. Specifically, a statistically modeled DFN, with numbers, total lengths, or average lengths of paths longer than certain thresholds similar to those of the field-collected fractures, will be eligible and selected for further analyses. If we fix our attention on the total paths ( $TL_{10}$ ,  $TL_{20}$ ,  $TL_{30}$ ,  $TL_{40}$ , and  $TL_{50}$ ), the results of DFNs 2, 9, 10, and 15 are close to those of field-collected fractures. Thus, four of the modeled 20 DFNs can be used for further analyses. Other fracture connectivity properties (e.g., total and average lengths) can also be considered, depending on the analysis requirement of engineering projects.

## 5.2 Influences of Length and Location Differences on Connectivity Discrepancies

Section 3 indicates that differences exist in fracture length and location distributions between field-collected and statistically modeled DFNs. The current section examines whether these differences will result in connectivity discrepancies in Sect. 5.1. We model two other types of DFNs with each type number 20 to implement this destination. One type of DFN only models fracture size (trace length) as shown in Sect. 2.3, with the fracture locations (midpoints) the same as the field ones. The other type of DFN only models fracture location, with the trace lengths stochastically selected from the field-collected fractures. Figure 13 exhibits the results of the number of paths  $N_1$  (e.g.,  $N_{1-10}$ ,  $N_{1-20}$ ,  $N_{1-30}$ ,  $N_{1-40}$ , and  $N_{1-50}$ ), total length of paths  $TL$  (e.g.,  $TL_{10}$ ,  $TL_{20}$ ,  $TL_{30}$ ,  $TL_{40}$ , and  $TL_{50}$ ), and average length of paths  $AL$  (e.g.,  $AL_{10}$ ,  $AL_{20}$ ,  $AL_{30}$ ,  $AL_{40}$ , and  $AL_{50}$ ) for different types of DFN.

Figure 13 shows that DFNs with field sizes have nearly the same  $N_1$ ,  $TL$ , and  $AL$  compared with the entirely modeled DFNs, which simultaneously model fracture size and position, as indicated in Sect. 2.3. Therefore, DFNs using field and modeled fracture traces nearly have no difference. In

other words, the discrepancy introduced in Sect. 3.1 is negligible in DFN applications. The connectivity discrepancy will be largely reduced, because differences in some trace lengths are limited compared with the long clustered fracture path. However, the discrepancy in fracture trace length distribution, which is discussed in Sect. 6, should still be considered in rock mass analyses.

The results in Fig. 13 indicate that DFNs with field locations have slightly deviated  $N_1$ , larger  $TL$ , and nearly the same  $AL$  compared with the entirely modeled DFNs. Thus, DFNs using field and modeled fracture locations yield differences. Difference in fracture locations introduced in Sect. 3.2 has an apparent effect on discrepancies in fracture connectivity and should thus be considered in DFN application. Specifically, DFNs with field locations have more concentration degree; thus,  $N_1$  (e.g.,  $N_{1-20}$ ,  $N_{1-30}$ ,  $N_{1-40}$ , and  $N_{1-50}$ ) values tend to be larger than those of totally modeled DFNs. However,  $N_{1-10}$  is smaller, because resulting in small paths with lengths ranging from 10 to 20 m for this degree of concentration is difficult. The other inclinations, which seem to be relatively difficult to understand, are explained as follows. Regular patterns are followed in the processes of fracture initiation, growth, interaction, and termination (Jing 2003; Welch et al. 2009; Bonneau et al. 2016). Geometric factors are randomly allocated to fractures via Monte Carlo simulation, as discussed in Sect. 2.3. Geometric characteristics of fractures in modeled DFNs (the three types of DFNs other than the field one) are more discrete. This finding results in a higher degree of connections among adjacent fractures than that for practically mechanically generated field fractures. Consequently, fractures in DFNs with field location distribution not only have the same concentration as the field DFN but also have the same connection as the entirely modeled DFNs. Therefore, DFNs with field locations have the largest  $TL$ . Connections will reduce  $N_1$  compared with field

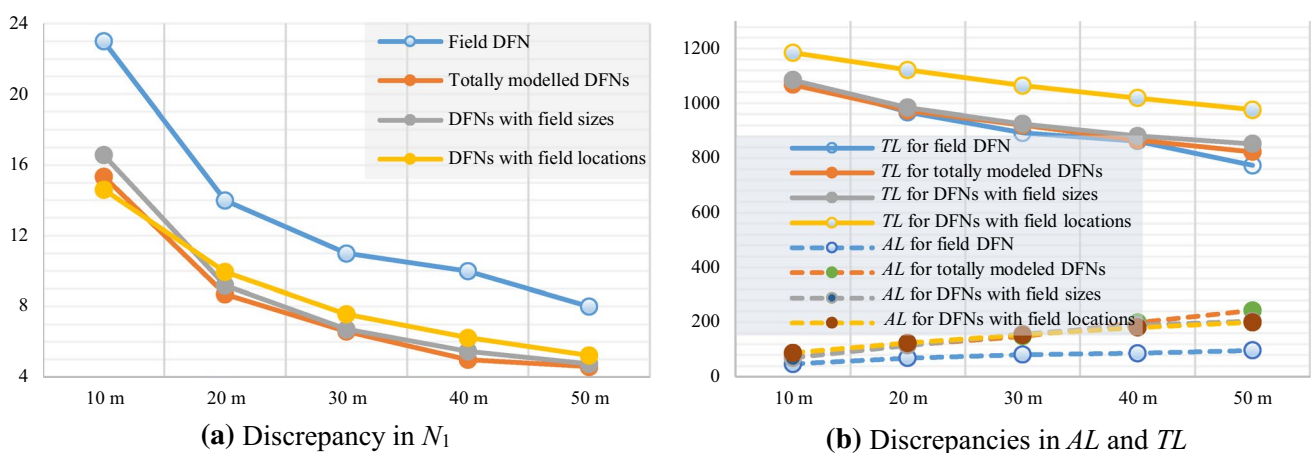


**Fig. 13** Discrepancies in  $N_1$ ,  $AL$ , and  $TL$  among field DFN, entirely modeled DFNs, DFNs with field sizes and DFNs with field locations.  $N_1$  is number of paths,  $AL$  is average length of paths, and  $TL$  is total length of paths

DFN; thus, the field-collected fractures have the largest  $N_1$ . Nevertheless, this property has not altered the connected fracture numbers and lengths compared with the entirely modeled DFNs; thus,  $AL$  values are nearly the same as those of entirely modeled DFNs, which are larger than field DFN.

## 6 Discussion

Our study carried out 2D discrepancy analysis (mainly connectivity) given that obtaining field 3D fractures is impractical using current technologies. The results presented in this manuscript are indicative for 3D DFN modeling and application. Given that the fracture-collection area reflects sampling from a cross section of the 3D space, 3D discrepancies inevitably exist. 3D DFN modeling and application (e.g., connectivity) should consider the discrepancy conclusions derived from the 2D analysis. Distributions of trace lengths and regularity pattern of fracture locations should be given particular focus ahead of 3D DFN modeling. Notably, 2D fracture network tends to underestimate the conductivity compared with 3D realizations given that the connectivity of the 2D DFN is inferior to that of 3D one (Yao et al. 2019). Therefore, 2D results can be used for qualitative or preliminary quantitative analyses (Ozkaya and Mattner 2003; Tang et al. 2017). 3D analyses would be more accurate and rational for practical engineering projects than 2D results.

Modeled DFNs have been traditionally examined to determine whether their distributions of fracture size, density, orientation, and trace types (e.g., one end observable, two ends observable, and no end observable) are statistically identical to those of field-collected fractures (Chen et al. 1995; Zhang et al. 2013). In this study, the traditionally used parameters are insufficient. Some studies have earlier mentioned the importance of using rock mass properties for DFN verification (Hestir and Long 1990; Xu et al. 2006). Considering other characteristics, such as fracture connectivity, will inevitably complicate the modeling processes, especially when statistical analyses are rational based on a large number of DFN analyses (Esmaili et al. 2010; Zhang et al. 2013). However, this complicated procedure is essential, because improvement of modeling accuracy is our fundamental purpose. The following paragraphs will focus on examining these discrepancies.

Although discrepancy in fracture trace length distribution is proven to have no effect on connectivity, as discussed in Sects. 3.1 and 5.2, this discrepancy remains enlightening for rock mass analyses, because further complicated cases may occur. For example, if we extend the research scope of fracture trace lengths to those shorter than 0.3 m, then, the fracture number will be highly increased (Wang and Sun 1990; Anders et al. 2014). Consequently, a single PDF cannot describe the practical trace lengths. As discussed in

Sect. 3.1, conventionally used distributions inevitably result in a large discrepancy and thus will no longer be applicable. Therefore, multi-distribution curves, which are more complicated than traditional means, may be more rational. In addition, the Chi-square and KS goodness-of-fit tests consider the trace length population including extremely large ones to derive PDF curves. Extremely large trace lengths, which are frequently collected in the field, will increase the mean and especially the deviation variance, making statistically modeled values deviate from field-collected ones for small trace lengths. We thus recommend that extremely large trace lengths, which could influence the precision of modeled PDF in terms of field fracture distribution, be separated from statistical analysis and then added into the accomplished DFN. Generally, differences between practical and statistical trace length distributions should be considered in DFN applications.

From the view of MSS, the way in which fractures distribute is contradictory to the traditionally used Poisson model, which results in noticeable connectivity discrepancies. We use a two-point correlation function  $C_2(r)$  to verify this conclusion as

$$C_2(r) = \frac{1}{N_2} N_d(r) \approx r^{D_c}, \quad (3)$$

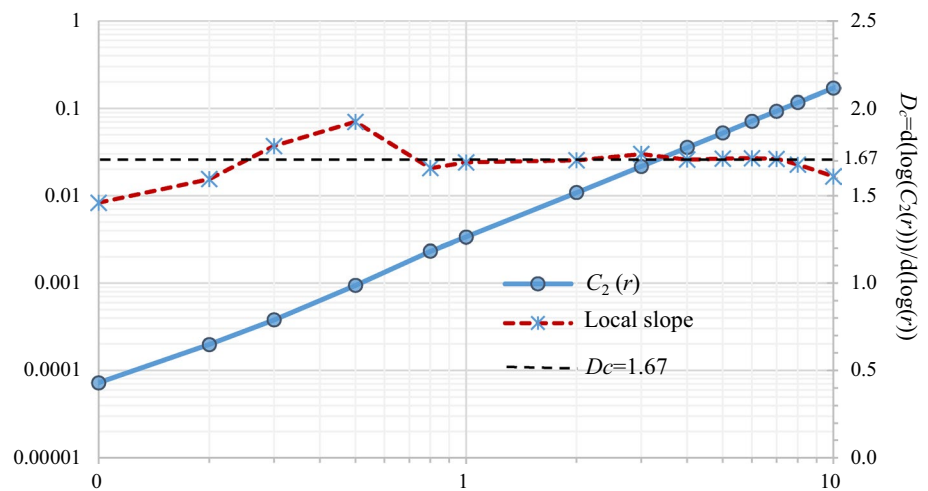
where  $D_c$  is the correlation dimension,  $N_2$  is the total number of the collected fracture traces, and  $N_d$  is the number of trace pairs whose distance of midpoints is smaller than  $r$ .

The two-point correlation dimension was calculated as 1.67 using Eq. (3). Figure 14 presents the result. Therefore, the fracture trace locations build a correlated DFN characterized by a correlation dimension inferior to 2. This result verifies that many fractures concentrate to each other, which is identical to the MSS pattern. We should alter the fracture location distribution in DFN modeling, which subsequently influences DFN applications in rock mass projects. Although some scholars have noticed the deficiency of the Poisson model for fracture locations and proposed many other methods (Davy et al. 2013; Bonneau et al. 2016), existing research is insufficient and has not been proven to be adequately relational. Fracture point process may not be homogeneous, which is contrary to the common conception that fractures in a rock mass with identical properties are homogeneously distributed. In addition, although the discrepancies may be reduced if MSS or correlation dimension was considered in this study, the discrepancies cannot be eliminated entirely, as shown in Fig. 13. Mechanical considerations for fracture locations may be indicative, which will be discussed in the last paragraph.

Our discrepancy tendencies are contrary to those derived from Odling (1992), which presented that natural fractures contained roughly half the number of clusters, and the longest



**Fig. 14** Calculation results of two-point correlation dimension for fracture trace locations according to Eq. (3).  $r$  extends from 0.1 to 10 m, and  $D_c$  is derived as 1.67



path was approximately double that of the realizations. We ascribe these contradictions to the difference in natural fracture patterns. Many natural fractures in the study of Odling (1992) are parallel, thereby resulting in low opportunities of connections among adjacent fractures even if cluster property is still manifested. Therefore, although discrepancy between field-collected and statistically modeled DFNs exists, the discrepancy inclinations may vary in terms of natural fracture patterns.

Section 5 implies that no matter which fracture geometric factor is altered to be the same as that in field, connectivity results can scarcely coincide with the outcomes determined on the basis of field-collected fractures. Therefore, we can only attempt to select certain DFNs with similar connectivity properties. This phenomenon is caused by the fractures with mechanical connections and are not geometric random objects. Therefore, DFN modeling with additional mechanical considerations is plausible (Lei et al. 2015; Bonneau et al. 2016; Li et al. 2018). However, the current research focuses on the initiation and propagation of limited fractures (Wong and Einstein 2009; Lee and Jeon 2011; Liu and Wang 2018), which practically represent large-scale ruptures in geological mass rather than stochastically distributed structural fractures. Researching regular patterns of location and geometric factors of a large number of structural fractures has profound importance in DFN modeling and application. Our study focuses on the problems in DFN modeling and application rather than solving them. Working on additional engineering projects and other rock mass properties is crucial to study the discrepancies and yield corresponding solutions.

## 7 Conclusion

This study takes sluice foundation rock mass in Datengxia Hydropower Station, China as an example and focuses on discrepancies in fracture geometric factors and connectivity between field-collected and statistically modeled DFNs. The findings are summarized as follows:

1. Many aspects that can lead to discrepancies in fracture geometric factors between field-collected and statistically modeled DFNs require consideration. For example, a PDF curve should be checked whether it is qualified to be representative of a factor distribution. Moreover, field-collected fractures are concentrated to one another rather than following a homogeneous (Poisson) model, as can be concluded from the mean, standard deviation, skewness, and excess kurtosis of the MSS PDF curves.
2. Remarkable discrepancies occur in rock mass properties (i.e., connectivity in this study) between field-collected and stochastically modeled DFNs due to differences in fracture location and distribution. Major inclinations of modeled DFNs tend to have small cluster numbers and long paths (applicable if path length thresholds are considered), which are indicative of low shear strengths of rock masses and large safety factors of engineering projects. Thus, discrepancies should be considered in DFN applications. In addition, the discrepancy tendencies are not fixed. Instead, they vary in terms of natural fracture patterns.

3. In view of rock mass properties, such as connectivity, selecting DFNs for application is essential. However, generating DFNs that resemble connectivity features of field-collected fractures is difficult. This difficulty is attributed to the mechanical connections of adjacent fractures, which cannot be reflected by geometric stochastic theories. Moreover, a focus on mechanical DFNs in future research is recommended.

**Acknowledgements** This work was supported by the National Nature Science Foundation of China (Grant numbers: 41877220 and 41472243), the National Nature Key Science Program Foundation (Grant number: 41330636), and the National Key Research and Development Plan (Grant number: 2017YFC1501000).

### Compliance with Ethical Standards

**Conflict of interest** The authors declare no conflict of interest.

### References

- Adler PM, Thovert JF, Mourzenko VV (2012) *Fractured porous media*. Oxford University Press, Oxford
- Anders MH, Laubach SE, Scholz CH (2014) Microfractures: a review. *J Struct Geol* 69:377–394
- Baghbanan A, Jing L (2008) Stress effects on permeability in a fractured rock mass with correlated fracture length and aperture. *Int J Rock Mech Min Sci* 45:1320–1334
- Bauer M, Toth TM (2017) Characterization and DFN modelling of the fracture network in a Mesozoic Karst Reservoir: Gomba Oilfield, Paleogene Basin, Central Hungary. *J Petrol Geol* 40:319–334
- Belayneh MW, Matthäi SK, Blunt MJ, Rogers SF (2009) Comparison of deterministic with stochastic fracture models in water-flooding numerical simulations. *AAPG Bull* 93:1633–1648
- Bondy A, Murty U (2010) *Graph theory (graduate texts in mathematics)*. Springer, London
- Bonneau F, Caumon G, Renard P (2016) Impact of a stochastic sequential initiation of fractures on the spatial correlations and connectivity of discrete fracture networks. *J Geophys Res Sol Ea* 121:5641–5658
- Bonnet E, Bour O, Odling NE, Davy P, Main I, Cowie P, Berkowitz B (2001) Scaling of fracture systems in geological media. *Rev Geophys* 39:347–383
- Chen JP, Xiao SF, Wang Q (1995) *Three dimensional network modelling of stochastic fractures*. Northeast norm University Press, Changchun
- Chen JP, Shi BF, Wang Q (2005) Study on the dominant orientations of random fractures of fractured rock mass. *Chin J Rock Mech Eng* 24:241–245
- Davy P, Goc RL, Darcel C (2013) A model of fracture nucleation, growth and arrest, and consequences for fracture density and scaling. *J Geophys Res Sol Ea* 118:1393–1407
- Einstein HH, Veneziano D, Baecher GB, Oreilly KJ (1983) The effect of discontinuity persistence on rock slope stability. *Int J Rock Mech Min Sci Geomech Abstr* 20:227–236
- Elmo D, Stead D, Eberhardt E, Vyazmensky A (2013) Applications of finite/discrete element modeling to rock engineering problems. *Int J Geomech* 13:565–580
- Elmo D, Rogers S, Stead D, Eberhardt E (2014) Discrete fracture network approach to characterise rock mass fragmentation and implications for geomechanical upscaling. *Min Tech* 123:149–161
- Esmaili K, Hadjigeorgiou J, Grenon M (2010) Estimating geometrical and mechanical REV based on synthetic rock mass models at Brunswick Mine. *Int J Rock Mech Min Sci* 47:915–926
- Fang JL, Zhou FD, Tang ZH (2017) Discrete fracture network modelling in a naturally fractured carbonate reservoir in the Jingbei Oilfield, China. *Energies* 10:183
- Grenon M, Hadjigeorgiou J (2003) Open stope stability using 3D joint networks. *Rock Mech Rock Eng* 36:183–208
- Han XD, Chen JP, Wang Q, Li YY, Zhang W, Yu TW (2016) A 3D fracture network model for the undisturbed rock mass at the Songta Dam Site based on small samples. *Rock Mech Rock Eng* 49:611–619
- Hao YH, Yeh TJ, Xiang JW, Lllman WA, Ando K, Hsu KC, Lee CH (2008) Hydraulic tomography for detecting fracture zone connectivity. *Ground Water* 46:183–192
- Hestir K, Long JCS (1990) Analytical expressions for the permeability of random two-dimensional Poisson fracture networks based on regular lattice percolation and equivalent media theories. *J Geophys Res* 952(B13):21565–21581
- Hudson JA, Harrison JP (1997) *Engineering rock mechanics: an introduction to the principles*. Pergamon, London
- Jayaram N, Baker JW (2008) Statistical tests of the joints distribution of spectral acceleration values. *B Seismol Soc Am* 98:2231–2243
- Jing L (2003) A review of techniques, advances and outstanding issues in numerical modelling for rock mechanics and rock engineering. *Int J Rock Mech Min Sci* 40:283–353
- Kulatilake PHSW, Wu TH (1984) Estimation of mean trace length of discontinuities. *Rock Mech Rock Eng* 17:215–232
- Kulatilake PHSW, Wu TH, Wathugala DN (1990) Probabilistic modelling of joint orientation. *Int J Numer Anal Methods Geomech* 14:325–350
- Kulatilake PHSW, Wang LQ, Tang HM, Liang Y (2011) Evaluation of rock slope stability for Yujian River dam site China by block theory analyses. *Comput Geotech* 38:846–860
- Lee H, Jeon S (2011) An experimental and numerical study of fracture coalescence in pre-cracked specimens under uniaxial compression. *Int J Solids Struct* 15:979–999
- Lee JS, Veneziano D, Einstein HH (1990). Hierarchical fracture trace model. In: Hustrulid, W., Johnson, G.A. (Eds.), *Rock mechanics contributions and challenges; Proceedings of the 31st US Rock Mechanics Symposium*, Balkema, Rotterdam, pp. 261–268
- Lei Q, Latham JP, Tsang CF, Xiang J, Lang P (2015) A new approach to upscaling fracture network models while preserving geostatistical and geomechanical characteristics. *J Geophys Res: Sol Ea* 120:4784–4807
- Li MC, Han S, Zhou SB, Zhang Y (2018) An improved computing method for 3D mechanical connectivity rates based on a polyhedral simulation model of discrete fracture network in rock masses. *Rock Mech Rock Eng* 51:1789–1800
- Liu J, Wang J (2018) Stress evolution of rock-like specimens containing a single fracture under uniaxial loading: a numerical study based on particle flow code. *Geotech Geol Eng* 36:567–580
- Liu Y, Wang Q, Chen JP, Song SY, Zhan JW, Han XD (2018) Determination of geometrical REV's based on volumetric fracture intensity and statistical tests. *Appl Sci* 8:800
- Malinuskaya I, Thovert JF, Mourzenko VV, Adler PM, Shekhar R, Agar S, Rosero E, Tsenn M (2014) Fracture analysis in the Amellago outcrop and permeability predictions. *Petrol Geosci* 20:93–107
- Odling NE (1992) Network properties of a two-dimensional natural fracture pattern. *Pure Appl Geophys* 138:95–114

- Odling NE, Webman I (1991) A “conductance” mesh approach to the permeability of natural and simulated fracture patterns. *Water Resour Res* 27:2633–2643
- Ozkaya S, Mattner J (2003) Fracture connectivity from fracture intersections in borehole image logs. *Comput Geosci-UK* 29:143–153
- Priest SD, Hudson JA (1981) Estimation of discontinuity spacing and trace length using scanline surveys. *Int J Rock Mech Min Sci Geomech Abstr* 18:183–197
- Sisavath S, Mourzenko V, Genthon P, Thovert JF, Adler PM (2004) Geometry, percolation and transport properties of fracture networks derived from line data. *Geophys J Int* 157:917–934
- Song SY, Sun FY, Chen JP, Zhang W, Han XD, Zhang XD (2017) Determination of RVE size based on the 3D fracture persistence. *Q J Eng Geol Hydrogeol* 50:60–68
- Stacey TR, Armstrong R, Terbrugge PJ (2015) Experience with the development and use of a simple DFN approach over a period of 30 years. *Min Tech* 124:178–187
- Tang YB, Li M, Li XF (2017) Connectivity, formation factor and permeability of 2D fracture network. *Phys A* 483:319–329
- Thovert JF, Adler PM (2004) Trace analysis for fracture networks of any convex shape. *Geophys Res Lett* 31:L22502
- Thovert JF, Mourzenko VV, Adler PM, Nussbaum C, Pinetters P (2011) Faults and fractures in the Gallery 04 of the Mont Terri rock laboratory: characterization, simulation and application. *Eng Geol* 117:39–51
- Thovert JF, Mourzenko VV, Adler PM, Nussbaum C (2014) Statistical analysis of the fracture network. In: Nussbaum C, Bossart P (eds) *Mont Terri Rock Laboratory*, 1st edn. Swisstopo, Wabern
- Vazaios I, Vlachopoulos N, Diederichs MS (2017) Integration of lidar-based structural input and discrete fracture network generation for underground applications. *Geotech Geol Eng* 35:2227–2251
- Vazaios I, Farahmand K, Vlachopoulos N, Diederichs MS (2018) Effects of confinement on rock mass modulus: a synthetic rock mass modelling (SRM) study. *J Rock Mech Geotech Eng* 10:436–456
- Wang CY, Sun Y (1990) Oriented microfractures in Cajon pass drill cores: stress field near the SAN Andreas Fault. *J Geophys Res* 95:135–142
- Welch J, Davies R, Knipe R, Tueckmantel C (2009) A dynamic model for fault nucleation and propagation in mechanically layered section. *Tectonophysics* 474:473–492
- White CD, Willis BJ (2000) A method to estimate length distributions from outcrop data. *Math Geol* 32:389–419
- Wong LNY, Einstein HH (2009) Systematic evaluation of cracking behavior in specimens containing single flaws under uniaxial compression. *Int J Rock Mech Min Sci* 46:239–249
- Wu X, Kulatilake PHSW, Tang HM (2011) Comparison of rock discontinuity mean trace length and density estimation methods using discontinuity data from an outcrop in Wenchuan area, China. *Comput Geotech* 38:258–268
- Xu CS, Dowd P (2010) A new computer code for discrete fracture network modelling. *Comput Geosci-UK* 36:292–301
- Xu C, Dowd PA, Mardia KV, Fowell RJ (2006) A connectivity index for discrete fracture networks. *Math Geol* 38(5):611–634
- Yang H, Shan RL, Zhang JX, Wu FM, Guo ZM (2018) Mechanical properties of frozen rock mass with two diagonal intersected fractures. *Int J Rock Mech Min Sci* 28:631–638
- Yao C, He C, Yang JH, Jiang QH, Huang JS, Zhou CB (2019) A novel numerical model for fluid flow in 3D fractured porous media based on an equivalent matrix-fracture network. *Geofluids* 2019:9736729
- Zhang W, Chen JP, Chen HE, Xu DZ, Li Y (2013) Determination of RVE with consideration of the spatial effect. *Int J Rock Mech Min Sci* 61:154–160
- Zhang W, Zhao QH, Huang RQ, Ma DH, Chen JP, Xu PH, Que JS (2017a) Determination of representative volume element considering the probability that a sample can represent the investigated rock mass at Baihetan Dam Site, China. *Rock Mech Rock Eng* 50:2817–2825
- Zhang W, Zhao QH, Chen JP, Huang RQ, Yuan XQ (2017b) Determining the critical slip surface of a fractured rock slope considering preexisting fractures and statistical methodology. *Landslides* 14:1253–1263

**Publisher's Note** Springer Nature remains neutral with regard to jurisdictional claims in published maps and institutional affiliations.